# Fracture of fiber reinforced concrete slabs on grade

A.Meda & G.A.Plizzari
*Department of Civil Engineering, University of Brescia, Brescia, Italy*

V.Slowik
*Hochschule für Technik, Wirtschaft und Kultur Leipzig (FH), Leipzig, Germany*

ABSTRACT: Nonlinear fracture mechanics has been used for simulating the load-carrying behavior of steel fiber reinforced concrete floors on elastic bedding. In a numerical parametric study, influences of the fiber content, the slab thickness and the soil stiffness on the structural response of the slab under both service and ultimate conditions were studied. The material properties adopted for the numerical analyses have been determined by mean of wedge splitting tests. Results of structural tests available in the literature are in good accordance with the simulation results. Furthermore, experimental observations regarding the influence of plastic and glass fiber reinforcement on early age cracking are presented.

## 1 INTRODUCTION

After about 30 years of research efforts, the use of fiber reinforced concrete is still limited with respect to the great benefits that fibers offer to concrete performance (Reinhardt & Naaman 1999). Besides the fact that concrete is traditionally designed to resist compression while fibers become effective after tensile cracking, another reason for the limited use of fibers is the imbalance between theoretical and applied research (Rossi & Chanvillard 2000). In fact, research studies on structural applications of fiber reinforced concrete have become important only in the last ten years (Di Prisco & Toniolo 2000). As a consequence, while the mechanical properties of fiber reinforced concrete are relatively well known, methods for designing fiber reinforced concrete structures, for example, are still missing in design codes. Only recently, guidelines for designing steel fiber reinforced (SFRC) elements were proposed, for instance by RILEM TC 162-TDF (2000).

It should be pointed out that traditional reinforcement is so cheap that it can hardly be substituted by fibers in structural elements subjected to bending, at least not within the next few years. Different is the case of transverse reinforcement that requires labor-intensive work. Here steel fibers may play a major role in the close future (Failla et al. 2000).

One of the more interesting applications of SFRC are slabs on grade that are often used for industrial floors (Zollo & Hays, 1991; Silfwerbrand 2000). This is one of the very few applications where steel fibers may actually substitute conventional rein-

forcement allowing to save intensive labor and expensive reinforcing work. However, the more extensive usage of SFRC for floors requires modified design rules and, most likely, SFRC would be used more often if reliable and simple design recommendations were available.

Whereas steel fiber reinforcement influences the load carrying capacity of hardened concrete floors and limits the crack widths under concentrated loading, plastic or glass fiber reinforcement does not have a significant influence on the mechanical properties of concrete. Therefore, the resistance against external forces, especially concentrated loads, and stresses due to constraint caused by drying shrinkage and thermal expansion (Olesen & Stang 2000), may be influenced by steel fiber reinforcement only. Plastic and glass fibers, however, are useful in reducing early age cracking.

In a first section of the paper, results of investigations into the effects of fibers on early age cracking are presented. The fracture behavior of hardened concrete floors is dealt with in the subsequent section by using nonlinear fracture mechanics (NLFM) approaches. Finally, numerical NLFM results are compared with experimental results available in the literature.

## 2 FIBER REINFORCEMENT FOR REDUCING EARLY AGE CRACKING

A major problem in the concrete floor technology is early age cracking due to the so-called plastic or capillary shrinkage of the young concrete. It is

caused mainly by the capillary water transport out of the hardening concrete. The resulting cracks are located on the concrete surface and appear usually within the first 24 hours after casting. Although appropriate curing is an important part of state-of-the-art concrete technology, early age cracking is still one of the most common constructional defects.

For studying influences on early age shrinkage of cementitious materials, fiber Bragg grating (FBG) sensors have been used (Slowik et al. 1998). This comparably new measuring technique is based on strain sensors "burned" into the glass core of tele-communication fibers. They provide an excellent long-term stability of strain measurements and may therefore be used efficiently for structural monitoring. Furthermore, the small dimensions of fiber Bragg gratings allow their utilisation for "microsensors" opening new fields of application in material science.

Taking advantage of the small sensor dimensions, experiments for characterizing the early age shrinkage behavior of cement paste were undertaken. By means of conventional methods it is technically difficult to measure shrinkage strains of cement paste in the early age (i.e. between 0 and 12 hours after mixing), since strain or displacement gauges cannot be attached before a certain minimum strength has been reached. Therefore, most measurements of shrinkage strains documented in the literature were carried out starting from the time of demoulding. If fiber-optics based microsensors are embedded in the fresh concrete, they start to monitor the strains immediately after the beginning of the setting. A slip between the fiber and the surrounding matrix does not occur due to the low fiber stiffness and the long grip length when compared to the fiber diameter.

Prismatic cement paste specimens having dimensions of 90x30x30 mm were cast into a form made of very flexible foamed plastics. The glass fiber containing a FBG sensor was embedded along the longitudinal axis of the specimen. A layer of impermeable foil placed between the form and the cement paste served to prevent water transport into the form. Yet drying was possible on the upper surface of the sample.

Figure 1 exhibits a typical shrinkage curve. About two hours after mixing, the shrinkage starts and strongly increases until an age of about 6 hours is reached. This is the time period between the beginning and the end of the setting. Simultaneously performed needle penetration tests confirmed this conclusion. After the period characterized by the high shrinkage strains, a volume increase could be observed for all the samples. This is predominantly caused by thermal expansion. Using embedded thermo-couples, a temperature increase of 10 K to 15 K could be determined at this age explaining the observed positive strain. The continuing deformation is due to drying shrinkage and yields toward an as-

ymptotic value. For the same sample, after three weeks the total strain amounted to -2700 μm/m for 20°C and 40% air humidity.

If the surface of the sample was sealed in order to prevent the water transport out of the specimen the shrinkage strain after 6 hours amounted to about 30% of the value measured in the unsealed specimens (Figure 2). The strain occurring in the sealed specimens is attributed to the chemical shrinkage. It was also shown that, by covering the specimen with an impermeable foil for the first 24 hours, the shrinkage strain occurring after a week is still significantly lower than in the case of no covering.
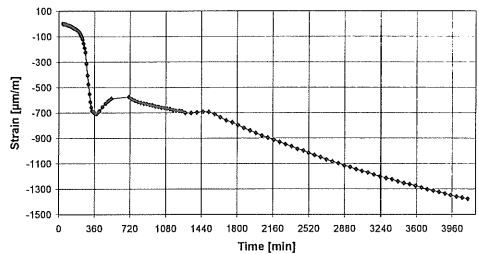


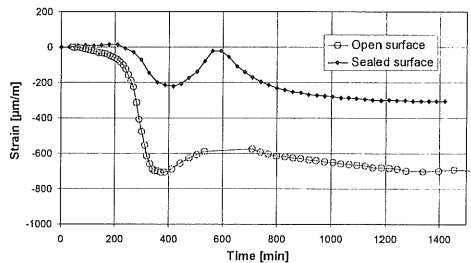Figure 1. Early shrinkage strain of cement paste, starting from the time of mixing, *w/c*-ratio 0.45.



Figure 2. Shrinkage strain of cement paste, *w/c*-ratio 0.45, open and sealed surface.

For a concrete with *w/c* ratio of 0.5, smaller early age shrinkage strains were measured as compared to a *w/c* ratio of 0.45. This is caused by the formation of a thin layer of water on the surface providing a perfect curing to the fresh cement paste having the higher *w/c* ratio. An air flow applied to the specimen surface has a significant shrinkage increasing effect (Schlattner et al. 1999).

In the experiments, it was confirmed that the early age shrinkage of cementitious materials is a complex process with a variety of different influences. Small variations in the composition of the cement paste or in the curing conditions might have significant effects on the shrinkage behavior. The prediction of the resulting early age cracking appears to be even more complicated. In addition to the unhindered shrinkage strain, the varying fracture mechanics properties and the creep behavior of con-

crete in the early age have to be known. The analysis of early age cracking, therefore, would require a number of assumptions to be verified in complicated experimental investigations into the individual physical effects having an influence on this complex process. It seemed to be more efficient to investigate early age cracking directly in structural tests performed under well defined conditions.

For investigating the effect of fiber reinforcement on early age cracking, an experimental set-up was used which allowed to observe the crack patterns formed in restraining concrete rings (Figure 3). This type of specimens has proved before to be efficient for investigating self-straining problems. The radial metal-pieces control the fracture localization resulting in a higher number of individual cracks. Sets of three identical specimens were cast out of one batch and their upper surface was subjected to a constant air flow in order to promote cracking.
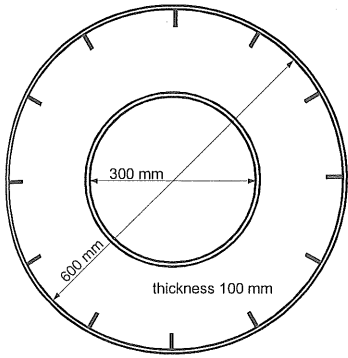


Figure 3. Restraining concrete ring for investigating early age cracking of concrete.

For a given concrete composition with a maximum aggregate size of 8 mm and a *w/c* ratio of 0.50, the influence of several types of plastic and glass fibers on early age cracking has been studied. In accompanying tests, early age shrinkage strains and fracture mechanics properties were determined. The fiber contents applied ranged from zero to 3 kg/m³.

It could clearly be shown that this type of fiber reinforcement significantly restricts early age cracking. This is due to the crack bridging behavior of the fibers in the young concrete and, to a certain extent, to the adhesion of the water to the fibers during the setting process. The latter was confirmed by smaller early age shrinkage strains measured in the concrete containing plastic or glass fibers. As expected, no significant influence of the fibers on strength and softening behavior was found.

As far as the influence of the fiber amount is concerned, for several plastic and glass fiber products it was shown that a fiber content as low as 1 kg/m³ already has a significant effect on the observed crack patterns (Figure 4). For this comparably low fiber

content, the workability of the fresh concrete is only slightly affected.

The experiments have also shown that the major parameter controlling the effect of plastic or glass fibers on early age cracking is the number of individual fibers per unit volume. Table 1 contains the crack lengths measured in restraining concrete rings reinforced with the same glass fiber product but different lengths.
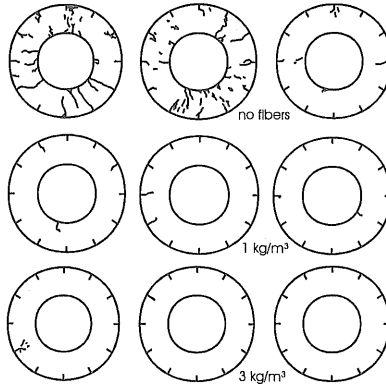


Figure 4. Crack patterns after 24 hours due to early age shrinkage of concrete containing glass fibers, fiber length 6 mm, fiber diameter 13 μm.

Table 1. Effect of the length of glass fibers on the early age crack length measured in three restraining concrete rings.

| fiber length | Fiber content | number of fibers | crack length |
|---|---|---|---|
| mm | kg/m³ | per m³ of concrete | mm |
| 6 | 1 | $0.570 \cdot 10^9$ | 113 |
| 12 | 1 | $0.285 \cdot 10^9$ | 318 |
| no fibers | - | - | 645 |

The numerous individual fibers act as a micro-reinforcement in the young cement paste transferring stresses and preventing fracture localization on this structural level. For a comparison, 30 kg/m³ of steel fibers having a length of 50 mm and an aspect ratio of 62.5 results in a fiber number of only $0,15 \cdot 10^6$ per cubic meter of concrete. For that reason, steel fibers are less effective for restricting early age cracking. However, they are useful for improving the mechanical behavior of hardened concrete.

## 3 NLFM ANALYSES OF SFRC PAVEMENTS

### 3.1 *Traditional design methods and advantages of using NLFM*

Traditional design methods for slabs on grade are based on the assumption that the slab remains elastic and uncracked under service loads. For this purpose, the elastic theory developed by Westergaard (1926)

may be applied. It is based on an elastic behavior of the slab and the subgrade is regarded as a Winkler soil where the pressure $p$ results from a linear elastic response varying with the slab deflection $w$ and being directly proportional to the modulus of subgrade reaction ($p=k\cdot w$). The required slab thickness results from the maximum tensile stress that needs to be smaller or equal to the concrete tensile strength ($f_{ct}$) reduced by the safety factor required by the design codes. However, the assumption of uncraked pavements is a simplification since cracks may also arise from shrinkage, thermal gradients or differential settlement of the subgrade.

An elastic approach is inappropriate for SFRC slabs since fibers do not have a significant influence on the concrete properties before cracking, so that the design based on an uncracked plate does not take advantage of the presence of the fibers. A suitable design method for SFRC slabs should consider the significant post-peak strength that characterizes steel fiber reinforced concrete (Figure 5). This can be achieved by performing a nonlinear fracture mechanics (NLFM) analysis (Hillerborg et al. 1976). In fact, when the maximum stress in the slab reaches the tensile strength ($f_{ct}$), because of the post-cracking concrete strength, the load might still increase while the crack propagates.
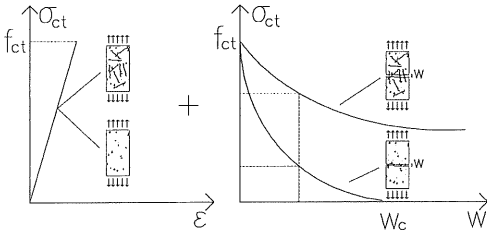


Figure 5. Pre-peak and post-peak behavior of plain and steel fiber reinforced concrete, respectively.

The analysis of a cracked structure leads to the need for a redefinition of slab failure and modified design requirements for both ultimate and service conditions.
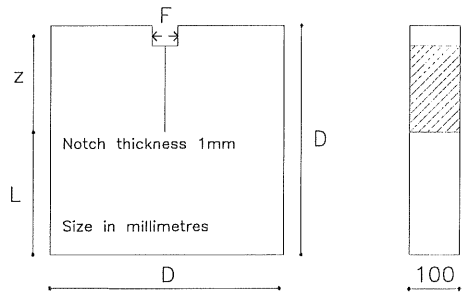
## 3.2 Experimental determination of fracture properties of SFRC

For determining the softening behavior of SFRC, wedge splitting tests were performed (Linsbauer & Tchegg 1986, Brühwiler & Wittmann 1990) on specimens having different sizes (Figure 6). The three different ligament lengths used (107 mm, 160 mm and 240 mm, respectively), are similar to the slab thickness often used for concrete floors.

For making the notches, 1 mm thick steel plates were placed in the wooden form. The specimens were demolded 24 hours after casting and the subse-

quent curing took place in a fog room at $20\pm1°C$ for at least 90 days in order to minimize the strength gain due to aging between the tests.

Four different mixes were prepared. Two of them are referred to here: a reference normal strength concrete (NSC) and a concrete with the same matrix but with 30 kg/m$^3$ (volume fraction = 0.38%) of steel fibers (NSC-SFR). Cement class 32.5 R type CEM II/B - L (UNI-ENV 197) was used as well as siliceous aggregates having a rounded shape, a maximum size of 15 mm and a grain size distribution very close to the Bolomey curve. The hooked steel fibers were cold drawn and 50 mm long. They had a diameter of 0.8 mm (aspect ratio=62.5) and a tensile strength higher than 1000 MPa (Figure 7).



| | D | L | z |
|---|---|---|---|
| Small | 200 | 107 | 73 |
| Medium | 300 | 160 | 120 |
| Large | 450 | 240 | 190 |

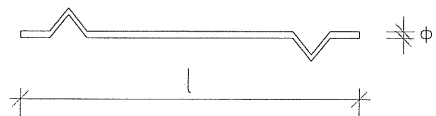Figure 6. Specimen geometry.



Figure 7. Hooked steel fiber geometry.

Table 2 shows the concrete composition, the compression strength measured from cubes ($f_{c,cube}$) at the time of testing (3 months). The workability of the fresh concrete, measured by the slump test, amounted to 160 mm for both plain concrete and fiber reinforced concrete.

Table 2. Composition and mechanical properties of concrete.

| Type | Cement [kg/m$^3$] | a/c | Aggr. [kg/m$^3$] | Fibers [kg/m$^3$] | $f_{c,cube}$ [MPa] |
|---|---|---|---|---|---|
| Plain | 300 | .53 | 1954 | - | 29.3 |
| SFRC | 300 | .53 | 1994 | 30 | 33.5 |

The specimens were suitably instrumented to measure the load and the crack mouth opening dis-

placement (CMOD) which was adopted as the feed-back quantity for the closed-loop control.

Softening laws for the two materials were approximated as bilinear laws (Figure 8) and determined by means of backward finite element analyses of the tests. These were performed by using FE code MERLIN (Reich et al. 1994) that is based on the discrete crack approach and uses the Fictitious Crack Model (FCM) proposed by Hillerborg et al. (1976).

Figure 9 shows typical load-CMOD curves as obtained on a medium size SFRC specimen. In the same figure, the best-fitting finite element curve is also plotted. The experimentally determined modulus of elasticity ($E_c$), uniaxial tensile strength ($f_{ct}$), and specific fracture energy ($G_F$) of concrete as well as the best-fitting parameters of the bilinear softening law are shown in Table 3.
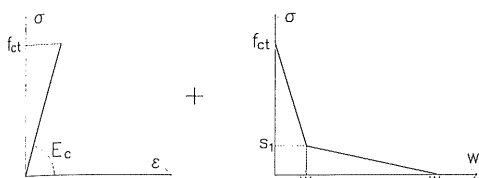


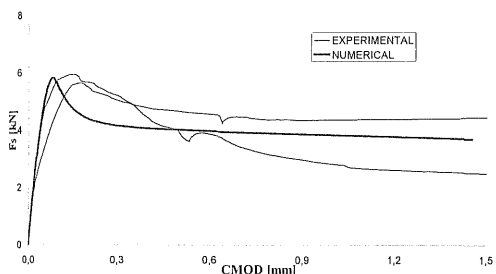Figure 8. Stress-strain curve and bilinear softening curve.



Figure 9. Typical experimental results, as obtained from the medium size wedge splitting specimens with steel fibers and the best fitting numerical simulation result.

Table 3. Fracture properties of concrete.

| Material | $E_c$ [MPa] | $G_F$ [N/m] | $f_{ct}$ [MPa] | $w_1$ [mm] | $s_1$ [MPa] | $w_c$ [mm] |
|---|---|---|---|---|---|---|
| NSC | 30000 | 0.21 | 2.72 | 0.024 | 0.896 | 0.406 |
| NSC-SFR | 34000 | 2.033 | 2.72 | 0.025 | 0.931 | 4.280 |

Further details on the experimental set-up as well as the complete set of experimental results can be found in Meda et al. (2001).

## 3.3 Numerical parametric studies

The experimentally determined fracture properties were adopted to simulate the deformation and cracking behavior of slabs with different thicknesses on subgrades characterized by different moduli. Two commercial programs utilizing different fracture mechanics approaches were used. Since the work was done independently by two teams, not all the input parameters were exactly the same.

Square slabs with an edge length of 5.0 m (typical for the distance between pavement joints), subjected to a centric load distributed in a square area ($a = 380$ mm), were modeled and analyzed (Figure 10).
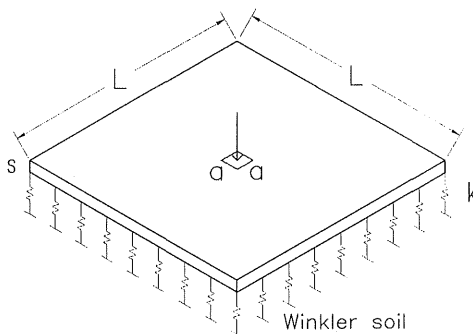


Figure 10. Model used for the numerical simulation by using MERLIN.

In parallel, 3D analyses of elastically supported concrete slabs under concentrated load were performed by using the program ATENA (Cervenka 2000) which is based on the smeared crack approach. An exponential softening law proposed by Hordijk (1991) has been applied for three different materials: plain concrete and fiber reinforced concrete with 20 and 30 kg/m³ of steel fibers, respectively. Because of the applied softening curve it was not possible to directly adopt the softening parameters from Table 3. The modulus of elasticity and tensile strength were kept constant and amounted to 30000 N/mm² and 2.72 N/mm², whereas the fracture energy was 0.15 N/mm, 0.25 N/mm and 0.30 N/mm, respectively, for the three materials. As in the case of MERLIN, a plate of 5.0x5.0 m was modeled. For the support, elastic brick elements were used in ATENA. Figure 11 shows a deformed 3D mesh of the slab. The concentrated load was applied in the center of the plate on an area of 125x 125 mm in this model.



Figure 11. Deformed finite element model of an elastically supported slab under concentrated load as obtained with ATENA.

Figure 12 exhibits the load-displacement curves obtained by using ATENA for different materials and a plate thickness of 160 mm. The supporting 400 mm thick layer had a modulus of elasticity of 165 N/mm$^2$. A corresponding result obtained by MERLIN for a slab thickness of 200 mm may be seen in Figure 13. All the numerical curves resulting from MERLIN are plotted up to the formation of the collapse mechanism that corresponds to the formation of cracks at the top surface of the slab. Even though the subgrade modulus used in ATENA is higher and the slab thickness is smaller than the corresponding values used in MERLIN, both analyses point to the same conclusion. There is only a slight influence of the fiber reinforcement even after the begin of cracking. The latter may be identified by the declining slope of the load-displacement curves. As already found by Falkner et al. (1995), only a small load increase results from the addition of usual volume fractions of steel fibers which, however, are useful in resisting shrinkage and thermal loading. The results also show the importance of a NLFM analysis that leads to a significantly higher loading capacity as compared to the elastic limit load which marks the beginning of cracking.
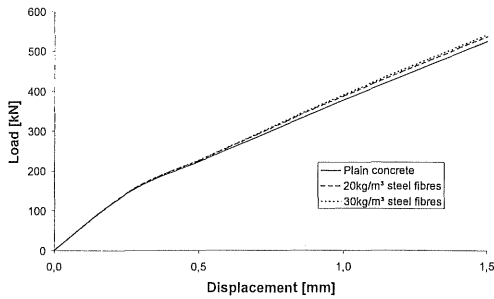


Figure 12. Load versus vertical displacement as obtained by ATENA for slabs of plain and steel fiber reinforced concrete.
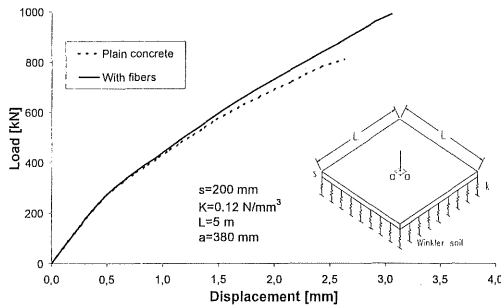


Figure 13. Load versus vertical displacement as obtained by MERLIN for slabs of plain and SFR concrete (30 kg/m$^3$).

The load-crack opening curves confirm that the steel fibers reduce the crack opening (Figure 14). This effect of the fibers is more significant and from a practical design point of view more important than the load increase for a given vertical displacement.

Figure 15 shows the load-displacement curves for SFRC slabs with different thicknesses on a subgrade with a modulus of 0.12 N/mm$^3$. For the same slabs, Figure 16 shows the load versus the maximum crack opening. It can be noticed that the maximum load increase is relatively small when compared to the increase in slab thickness. However, referring to service conditions, if the maximum crack opening has to be limited, for example to 0.3 mm, the service load turns to be strongly dependent on the slab thickness (Figure 16).

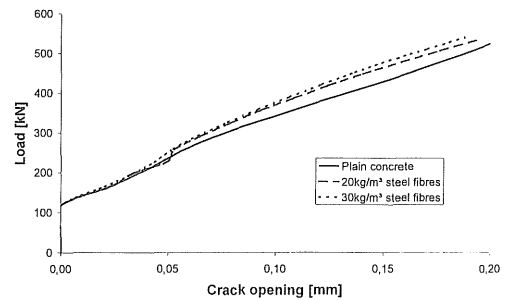The subgrade modulus has a significant influence



Figure 14. Load versus maximum crack opening as obtained by ATENA for slabs of plain and steel fiber reinforced concrete.
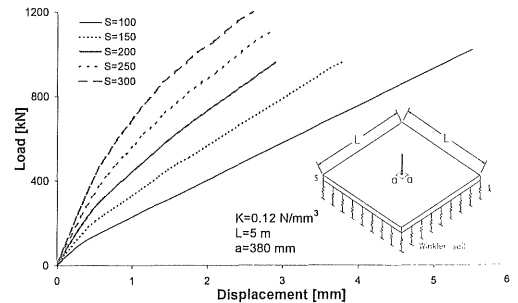


Figure 15. Load versus vertical displacement as obtained by MERLIN for slabs with different thickness.
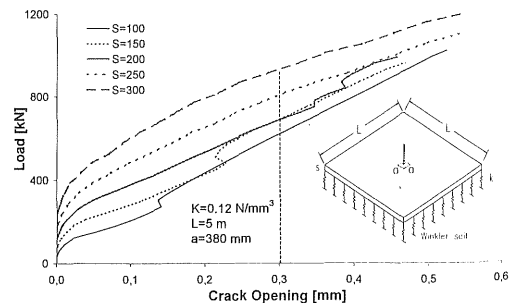


Figure 16. Load versus maximum crack opening as obtained by MERLIN for slabs with different thickness.
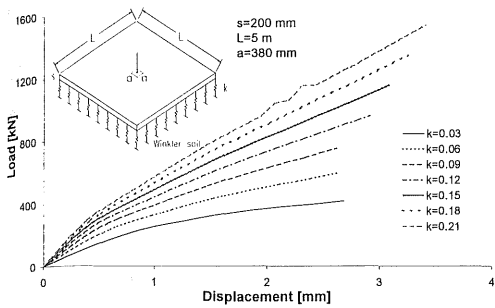
Figure 17. Load versus maximum crack opening as obtained by MERLIN for slabs on elastic subgrade having different moduli.

on the stiffness and the ultimate load of concrete slabs. This can be observed in Figure 17 that shows the load-displacement curves for a SFRC slab on subgrades having different moduli, ranging within values significant for practical applications. The numerical curves were obtained with MERLIN.

### 3.4 Comparison with experimental results

Experiments performed by Falkner et al. (1995) were analyzed by using MERLIN in order to verify the numerical model. Tests on 3.0x3.0x0.15 m concrete slabs centrally loaded on a 120x120 mm steel plate were carried out. Two specimens (P3 and P4) of normal strength concrete ($R_{ck} \approx 35$ MPa) reinforced with 20 kg/m³ of hooked steel fibers were considered here. The steel fibers had a minimum tensile strength of 1100 MPa, a length of 30 mm and a diameter of 0.8 mm (aspect ratio=37.5). The slabs were placed on 3.5x3.5x0.06 m bases. For specimen P3 a cork base ($k$=0.025 N/mm³) was used while a rubber base was adopted for specimen P4 ($k$=0.05 N/mm³).

Table 4 shows the experimentally determined modulus of elasticity ($E_c$), the compression strength ($f_c$) and the flexural strength ($f_{ctf}$) of concrete used for the slabs. The tensile strength ($f_{ct}$) was determined from the flexural strength according to EC2 (1991).

Table 4. Mechanical properties of concrete used by Falkner et al. (1995).

| | $E_c$ [MPa] | $f_c$ [MPa] | $f_{ctf}$ [MPa] | $f_{ct}$ [MPa] | $w_1$ [mm] | $s_1$ [MPa] | $w_c$ [mm] |
|---|---|---|---|---|---|---|---|
| P3 | 23400 | 37.5 | 3.76 | 2.60 | 0.04 | 1.058 | 5.01 |
| P4 | 26650 | 42.8 | 4.03 | 2.75 | 0.05 | 0.718 | 5.56 |

The concrete fracture properties were experimentally determined by means of four point bending tests performed on beams of the same materials used for the slabs (Falkner et al. 1995). For the analysis performed here, the softening laws had to be approximated by bilinear laws and were determined by

means of a backward finite element analysis of the beam tests. This was also done by using MERLIN. The parameters of the bilinear softening laws for the materials used in specimens P3 and P4 are summarized in Table 4. By using the actual material properties, finite element simulations of the structural behavior of specimens P3 and P4 were performed.

In the numerical model, the soil consisted of a set of springs (attached to all slab bottom nodes) representing the Winkler soil. The spring stiffness was set to represent the modulus of the base used in the experiments.

The comparison between numerical and experimental results, in terms of load versus vertical displacement, is shown in Figure 18. A good accordance between the two sets of curves can be observed up to the first peak load which marks the formation of a collapse mechanism. The latter is evidenced by the load decrease in the numerical curves but it is not seen in the experimental curves. In fact, because of the presence of steel fibers across the crack, the slab continues to carry the load because of the reaction of the subgrade. Furthermore, the friction between the continuous cork or rubber subbase and the concrete slab may have influenced the crack opening. This effect could not be simulated
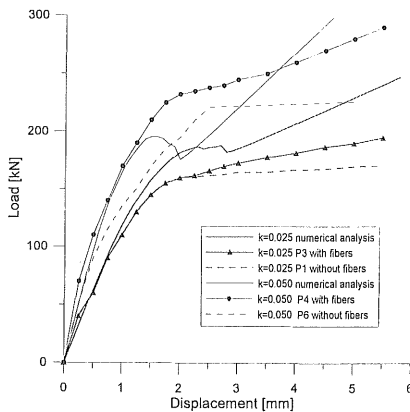


Figure 18. Comparison between the numerical and the experimental results obtained by Falkner et al. (1995).
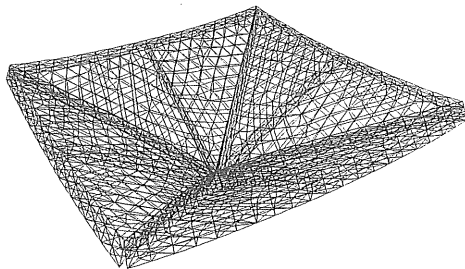


Figure 19. Deformed mesh of MERLIN at first peak load in slab P3.

by the independent springs (adopted to simulate the Winkler soil) used in MERLIN, and might explain the difference between the final parts of the two sets of curves where the load is mainly carried by the subgrade.

Figure 18 also shows the experimental curves obtained for the plain concrete slabs P1 ($k$=0.025 N/mm$^3$) and P6 ($k$=0.05 N/mm$^3$ (Falkner et al. 1995). It can be noticed that, with the adopted low fiber content, the ultimate loads of the plain concrete slabs are very close to the ones of the SFRC slabs. The deformed mesh at the first peak (collapse) load is shown in Figure 19.

## 4 CONCLUDING REMARKS

Slabs on grade are an appropriate application for steel fiber reinforced concrete. Under certain circumstances, the use of steel fibers can save expensive and time consuming reinforcing work.

The usage of steel fiber reinforcement requires the application of nonlinear fracture mechanics approaches for the analysis. In this way, the considerable post-cracking strength of the steel fiber reinforced concrete can be fully taken into consideration. The load-carrying capacity obtained by considering the post-cracking behavior of the structure is significantly higher than the one resulting from a traditional elastic analysis.

Whereas the influence of the steel fibers on the ultimate load is comparably small, there is a strong effect on the maximum crack openings. Therefore, the steel fiber reinforcement increases the allowable load under service load conditions.

Whereas steel fibers actually affect the mechanical behavior of concrete slabs, glass and plastic fibers have only a negligible influence on strength and softening parameters of the hardened material. However, even small quantities of such fibers added to the concrete mix significantly reduce early age cracking.

## REFERENCES

Brühwiler, E. & Wittmann, F.H. 1990. The wedge splitting test, a new method of performing stable fracture mechanic tests. *Engineering. Fracture Mechanics*, 35 (1/2/3): 117-125.

Cervenka Consulting 2000. ATENA Program Documentation. Prague May 2000.

Di Prisco, M. & Toniolo, G. Editors 2000. *Structural applications of steel fibre reinforced concrete. Proceedings of the international workshop. Milan, April 4.*

EC2 1991, EUROCODE No.2: Design of concrete structures - Part 1-1: General rules and rules for buildings. European Committee for Standardization. ENV 1992-1-1.

Failla, C., Toniolo, G. & Ferrara, L. 2000. Design criteria for structural use of fibre-reinforced concrete in prestressed precast roof elements. *Fifth RILEM Symposium on Fibre-Reinforced Concretes (FRC). Lyon, France, 13-15 September*: 253-262.

Hillerborg, A., Modèer, M. & Petersson, P.E 1976. Analysis of crack formation and crack growth in concrete by means of fracture mechanics and finite elements. *Cement and Concrete Research* 6: 773-782.

Hordijk, D.A. 2000. Local approach to fatigue of concrete. PhD thesis. Delft University of Technology, Netherlands.

Linsbauer, H.N. & Tchegg, E.K. 1986. Fracture energy determination of concrete with cube-shaped specimens. *Zement und Beton*. 31: 38-40.

Meda, A., Plizzari, G.A., Ferrari, K., Gregorelli, M., Minelli, F. & Zwerger, J. 2001. Studio sul comportamento a frattura di piastre per pavimentazione in calcestruzzo fibrorinforzato, Technical Report, Dept. of Civil Eng., Univ. of Brescia.

Olesen, J.F. & Stang, H. 2000. Designing FRC slabs on grade for temperature and shrinkage induced cracks. *Fifth RILEM Symposium on Fibre-Reinforced Concretes (FRC). Lyon, France, 13-15 September*: 337-346.

Reich, R., Cervenka, J. & Saouma, V.E. 1994. *MERLIN, a three-dimensional finite element program based on a mixed-iterative solution strategy for problems in elasticity, plasticity, and linear and nonlinear fracture mechanics.* Palo Alto (CA): EPRI. Vol. I Mesh Generator's Manual; Vol II User's Manual; Vol. III Example's Manual; Vol. IV Programmer's Manual; Vol. V Theory Manual.

Reinhardt, H.W. & Naaman, A.E. Editors 1999. *High performance fiber reinforced cement composites-HPFRCC 3. RILEM PRO 6.* Cachan (Fr): RILEM Publications S.A.R.L.

RILEM TC 162-TDF 2000. Test and design methods for steel fibre reinforced concrete-Recommendations. *Materials and Structures*. 33: 75-81.

Rossi, P. & Chanvillard, G. Editors 2000. *Fifth RILEM Symposium on Fibre-Reinforced Concretes (FRC). Lyon, France, 13-15 September.*

Schlattner, E., Slowik, V. & Klink, T. 1999. Neue Möglichkeiten zur langzeitigen Dehnungsmessung im Bauwesen mittels Faser-Bragg-Gitter-Sensoren. *Bautechnik* 76 (10): 884-887.

Silfwerbrand, J. 2000. Design of steel fibre reinforced slabs on grade. *Fifth RILEM Symposium on Fibre-Reinforced Concretes (FRC). Lyon, France, 13-15 September*: 305-314.

Slowik, V., Schlattner, E. & Klink, T. 1998. Strain monitoring at concrete structures by using fibre Bragg grating sensors. In P. Schwesinger, F.H. Wittmann (ed.), *Durable Reinforced Concrete Structures 5th Internat. Workshop on Material Properties and Design, Weimar, Germany, Oct. 29-30 1998*: 477- 493. Freiburg: AEDIFICATIO.

Westergaard, H.M. 1926. Stresses in concrete pavements computed by theoretical analysis. *Public Roads*. 7(2): 25-35.

Zollo, R.F. & Hays, C.D. 1991. Fibers vs. WWF as nonstructural slab reinforcement. *Concrete International*, November: 50-55.